Tanzania Journal of Science 50(4): 884-897, 2024
ISSN 0856-1761, e-ISSN 2507-7961

Exploring Dependence of Rapid Thermal Annealed Ag/ITO Bilayer Films Properties on the Systematic Ag Layer Thickness Increment for Bifacial CZTS Solar Cell Application

Emmanuel R Ollotu[1,*], Justine Nyarige[3], Margaret E Samiji[2], Nuru R Mlyuka[2], Mmantsae Diale[3]

[1]Department of Mathematics, Physics and Informatics, Mkwawa University College of Education, P.O. Box 2513, Iringa, Tanzania

[2]Departments of Physics, University of Dar es Salaam, P.O. Box 35063, Dar es Salaam, Tanzania

[3]Department of Physics, University of Pretoria, Private Bag X20, Hatfield, 0028, South Africa

**E-mail: emmanuel.ollotu@udsm.ac.tz; emmanuel.ollotu@muce.ac.tz; manyoolo@gmail.com*

Received 8th Aug. 2024, Reviewed 30th Aug., Accepted 27th Oct., Published 30th Nov. 2024

https://dx.doi.org/10.4314/tjs.v50i4.14

Abstract

This study investigated the impact of Ag layer thickness on the properties of rapid thermal annealed Ag/ITO bilayer films, aimed at addressing conductivity loss in ITO substrates used as a back contact for optoelectronic applications, such as bifacial CZTS solar cells. Ag layers of varying thickness (10 nm, 20 nm, 30 nm, and 40 nm) were sputter-deposited onto a commercially acquired ITO-coated glass substrate and rapidly thermally annealed. The samples' characterization was performed using AFM, XRD, four-point probe, Hall Effect measurements, and UV-VIS-NIR spectrophotometry. Results indicated that thinner Ag layers exhibited relatively stable surfaces with uniformly distributed grains, smaller roughness, and higher electrical conductivity due to increased carrier mobility and concentration. The XRD analysis showed a preferential delafossite $AgInO_2$ structure for thinner Ag layers. Optical measurements revealed that the sample with thinner Ag layers had lower solar transmittance and bandgap narrowing, while thicker layers showed bandgap broadening. The samples had bandgaps within reported ITO bandgaps (3.38 to 4.15 eV). Ag/ITO films with thinner layers achieved a high average transmittance of 76%, lower sheet resistance of $13.2\,\Omega/\square$ and enhanced micro-strain and crystallite size properties. These results suggest that thinner Ag/ITO bilayer films hold potential for use in optoelectronic applications, particularly as back contacts in bifacial CZTS solar cells.

Keywords: Ag/ITO properties; DC Sputtering; Rapid thermal annealing (RTA); Bifacial CZTS solar cells

Introduction

Indium Tin Oxide (ITO) is an established material for application in the optoelectronics field due to its outstanding optical and electrical properties (Granqvist 2007). Its optical properties reach as high as 90 % in the visible range and resistivity down $7.2\times10^{-5}\,\Omega\,cm$ (Granqvist and Hultåker 2002). These properties remain relatively higher than those of aluminium-doped zinc oxide (AZO) and fluorine-doped tin oxide (FTO) (Granqvist 2007). Therefore making ITO thin films attracts applications in several fields including organic light-emitting devices, liquid crystal displays, solar cells and many others (Guillén and Herrero 2006, Han et al. 2006, Song et al. 2011).

However, emerging processing conditions for materials grown on ITO-coated glass substrates mandate the substrate's properties further understanding. Because such processing can affect the properties of ITO properties differently. In particular, studies indicate that the ITO-coated substrate loses its conductivity during the thermal processing of a bifacial CZTS solar cell absorber grown on an ITO-coated glass substrate (Ge et al. 2015, 2016, Kim et al. 2016). Usually, the thermal processing is carried out at elevated temperatures above $500\,^{o}C$ causing the substrate conductivity to deteriorate thus affecting the bifacial device's efficiency. Besides, bifacial solar cell architecture can boost solar cell power since the architecture can harness solar energy from the front and rear sides of the solar cells (Kim et al. 2016). Using a CZTS absorber in bifacial solar cells makes the device even more potential as researchers consider the absorber to be cheap, earthly abundant and environmentally friendly (Cui et al. 2014, Ge et al. 2016).

Some approaches have been suggested to address the observed ITO conductivity loss problem during elevated temperature annealing. These include shortening thermal processing time through rapid thermal annealing (RTA). Applying a thin layer of highly conductive metal such as Ag has also been suggested (Cui et al. 2014). Concurrently employing the two suggested approaches can further address the conductivity loss problem. Besides, Ag use can benefit the precursors as it is reported to reduce the precursor's defects and improve grain size and the device performance (Mwakyusa et al. 2020).

A literature review indicated limited information on the dependence of a systematic incremental of Ag layer thickness on the annealed Ag/ITO bilayer film properties essentially those annealed rapidly. Conventionally annealed Ag/ITO sample with thicker Ag layer thickness, at elevated temperatures above $500\,^{o}C$ have indicated improved the sample's mean crystallite size and surface agglomeration and roughness (Guillén and Herrero 2015). Another similar study by Sivaramakrishnan et al. (2009) indicated enhanced samples' surface agglomeration and improved electrical stability with increased annealing temperature when Ag layer thickness increased (Sivaramakrishnan et al. 2009). Similar results were observed for the Ag layer grown on SiO_2 (Kim et al. 2002) and GaN (Lee et al. 2013). This study reports on the dependence of properties of rapid thermally annealed Ag/ITO bilayer films on the systematic incremental Ag layer thickness. The dependence can assist in the choice of appropriate Ag layer thickness to employ on the ITO-coated substrate for the proposed thermal processing conditions. The Ag layers of incremental thickness were sputtered on commercially acquired ITO-coated glasses using DC magnetron sputtering at room temperature. The fabricated and subsequently RTA Ag/ITO films indicated differing structural, electrical and optical properties. The Ag/ITO bilayer with a thinner Ag layer indicated potential properties for application in optoelectronics devices viz. bifacial CZTS solar cells' back contact.

Materials and Methods

Ag layers of incremental thickness were sputter deposited on commercially acquired ITO-coated glass and subsequently RTA at $550\,^{\circ}C$ to ascertain the dependence of the produced bilayers' film properties on the Ag thickness increments. The Ag/ITO bilayer films were deposited at room temperature from an Ag metallic planar disk target (diameter 50.8 mm thickness 6.35 mm and purity 99.99%) using DC magnetron sputtering. Before deposition, the ITO-coated glasses were ultrasonically cleaned in Deionized (DI) water for 25 minutes, air dried and fixed in the sputtering chamber, 15 cm above the target. The chamber was then evacuated to a base pressure of 5.8×10^{-6} mbar. Argon gas (purity 99.99 %) was allowed into the chamber at the rate of 50 sccm making the chamber attain a working pressure of 5.1×10^{-3} mbar. Using a sputtering power of 20 W at different controlled sputtering times, Ag/ITO bilayer

films of incremental Ag thickness, namely; 10 nm, 20 nm, 30 nm and 40 were deposited. The fabricated bilayer films were rapidly annealed in a rapid thermal processing unit (RTP 1000D4) furnace in nitrogen gas at $550\,^{\circ}\mathrm{C}$ for 5 minutes at a ramping rate of $20\,^{\circ}\mathrm{Csec}^{-1}$. The furnace quartz tube was evacuated using the rotary oil-sealed mechanical pump for 30 min, before allowing the nitrogen gas at 60 ml/min. Bare ITO-coated glass was also annealed under similar conditions for comparison.

The samples' properties were determined using relevant techniques as follows: The Ag layer thickness was measured using a surface profiler (KLA Tencor Alfa-step 200 IQ profilometer). The surface morphology of the samples was determined using atomic force microscopy (AFM) (Veeco Instrument, Nanoscope IIIa Multimode) operated in tapping mode using RTESP7, $125\,\mu m$ pyramidal silicon tips for a scan size of $1\times 1\,\mu m$ at a scan rate of $2\,Hz$. The grain size, distribution, and surface roughness were analysed from AFM images using the method detailed in our previous work (Ollotu et al. 2020). The structural properties of the bilayer films were determined by an X-ray diffractometer (XRD) (German Bruker D2 PHASER) with $CuK\alpha$ of radiation wavelength of 0.15406 nm generated at 30kV and 10 mA. The 2θ angle ranged from 20 to 80 at an interval of 0.04° and speed of $2^{\circ}/\mathrm{min}$ in a locked coupled scanning mode. The sheet resistance was determined using a four-point probe (Jandel Model 3R). The electrical conductivity, carrier concentration and mobility of the bilayer films were measured using a Hall Effect measurement system (HMS ECOPIA 3000) with a magnetic field of 0.56 Tesla and probe current of 1 mA. The transmittance of the bilayer films was assessed by UV/VIS/NIR spectrophotometer (Pekin Elmer Lambda 9/19) in the wavelength range of 250 nm - 2500 nm.

Results and discussion

Morphological properties

Compared to the rest of the samples, the AFM study showed, that the thinner Ag layer had relatively stable surface properties. The 10 nm Ag layer sample showed a surface with roundish small grains and limited bulging grain clusters (Figure 1 [a-b]). This hints at an onset of the sample surface to agglomerate. Surface bulging clusters were further enhanced by incrementing the sample's thicknesses to 20 nm (Figure 1 [d-e]). The bulging suggested that with annealing, this Ag layer thickness is further agglomerating developing the bulging features. Conversely, with the 30 nm Ag layer sample, the budging grains cluster surface that was observed for the 20 nm Ag layer sample disappeared (Figure 1 [g-h]). Instead, a sharper smaller grain surface was observed. Likely, at this Ag layer thicknesses, annealing had caused the sample to delaminate from ITO films leaving the sample's surface with the sharper gain features. This was different for the 40 nm Ag layer sample, where a total removal of the Ag layer is suggested, leaving a more uniform surface with only a few large protruding features (Figure 1 [j-k]). This result suggests that the present annealing conditions at this Ag layer thickness, caused a different Ag layer delaminating behaviour.

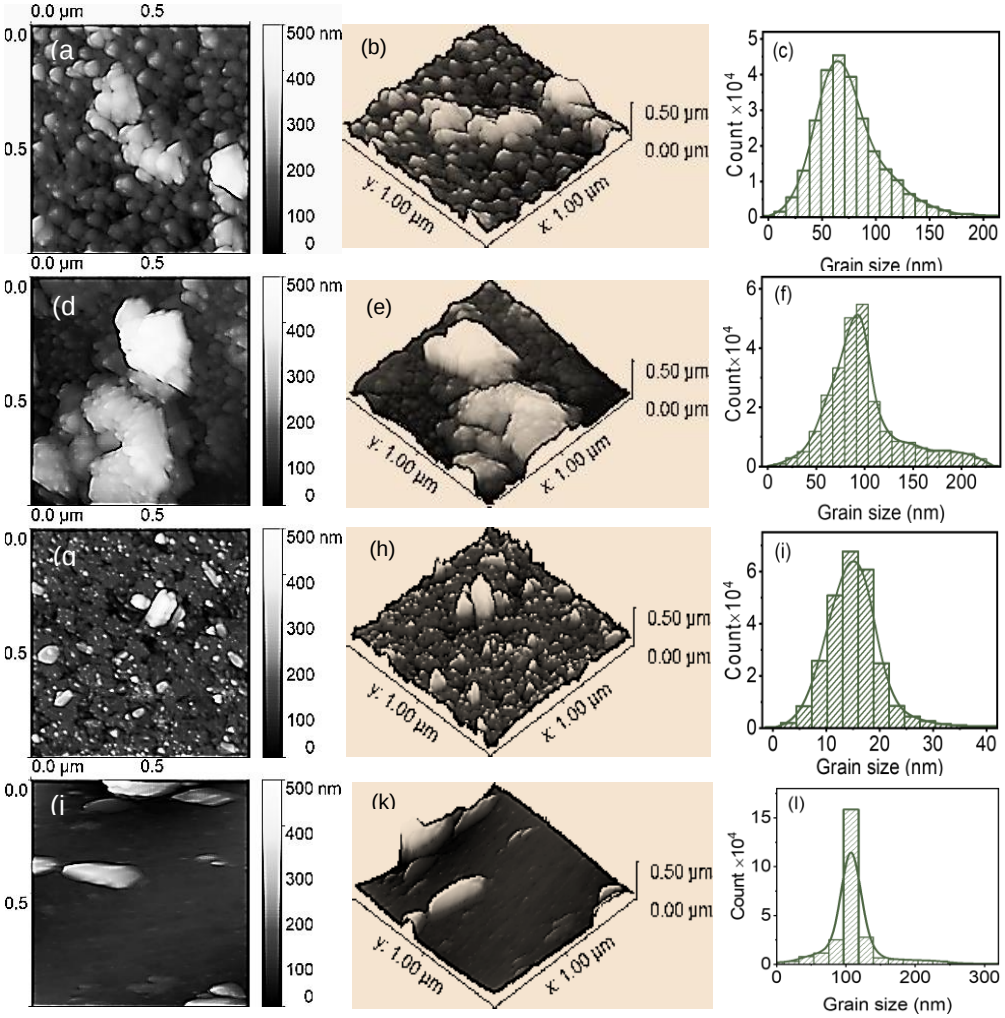

Figure 1: 2D and 3D AFM images and grain distribution for the 10 nm (a-c), 20 nm (d-f), 30 nm (g-i) and 40 nm (j-l) annealed Ag/ITO bilayer films of Ag layer thickness increment

Further AFM images analysis suggested that at the present annealing conditions, thinner Ag layer thickness can provide surfaces with relatively larger and uniformly distributed grains. (Table 2). Compared to the ITO sample, the 10 nm Ag layer sample indicated enhanced sample grain size and surface roughness. These changes suggested a diffuse of the Ag atoms into the ITO films which interrupted the homogeneity of the ITO, causing the grains to grow larger. This also created irregularities in the grain boundaries and surface, causing increased surface roughness. The slight decrease in skewness value for this sample relative to the ITO films suggested that the distribution is becoming more symmetric because more grains are becoming larger. The reduced kurtosis value relative to the ITO films suggested that the grain distribution became less peaked and more spread out (Figure 1 c). At the 20 nm Ag layer, the sample grain size continued to increase and surface roughness rose. At this thickness, Ag has begun to agglomerate, causing grains to coalesce, leading to larger but uneven grain sizes and an increase in roughness. Likely, these changes caused the distribution to become

asymmetric again, as the skewness value suggested (Table 1) forming larger grains while some smaller ones remained. The kurtosis also slightly decreased for this sample suggesting less picked distribution likely due to grain growth and more grain size variation during agglomeration.

A significant decrease in the grain size and roughness was observed for the 30 nm sample. This decrease can be attributed to the onset of delamination of the Ag layer from the ITO substrate causing the grains to fragment, reducing the overall size of the grains. The delaminated surface showed grains distributed asymmetrically with extremely peaked features, as the respective skewness and kurtosis values indicate (Table 2). When the Ag layer is 40 nm, the sample's grain size and surface roughness increased again which is larger than before. Likely at this Ag layer thickness, a larger layer of Ag is peeled off from the ITO surface. The remaining fragments of the films form larger isolated grains, resulting in very larger grain sizes in unlinked regions. The increased roughness can also be attributed to the irregular surface of the delaminated surface. The further increase in skewness indicates a further increase in asymmetric grain size distribution due to the observed larger grains in isolated areas (Figure 1). Whereas, the continued rising of kurtosis value indicated that the grains were even more peaked distributed, with fewer extremely large grains and many smaller grains. This means the samples were highly fragmented, with only a few larger grains remaining while the rest were broken down as suggested by the AFM images (Figure 1).

Table 1: Surface parameters for the annealed ITO and Ag/ITO bilayer films of Ag layer thickness increment

Ag thickness (nm)	Grain size (nm)	Roughness (Sa) (nm)	RMS (Sq) (nm)	Skewness (S_{sk})	Kurtosis (S_{ku})
0	12.7	2.85	3.77	1.19	7.85
10	80.6	23.7	31.0	0.936	4.34
20	104.8	28.2	39.0	1.06	4.19
30	16.9	3.99	5.85	1.89	11.3
40	124.4	20.7	39.5	1.99	13.0

Structural properties

The XRD analysis also indicated that the thinner Ag layer has a relatively higher potential to impact the ITO phase properties at the present annealing conditions relative to the thicker Ag layer. The 10 nm Ag layer sample showed the delafossite structure of $AgInO_2$ JCPDS card no. 21-1077 strong XRD peak (Figure 2). The peak was observed at $2\theta = 28.6^o$ corresponding to the (006) phase, which was also observed on annealed Ag content incorporated into ITO thin films (Mirzaee and Dolati 2014). Diffusing atoms of Ag into the ITO matrix through available oxygen vacancies or interstitials essentially for thinner Ag bilayer films might explain the existence of the delafossite phase. The phase however decreased with increasing Ag layer thickness and disappeared for 40 nm Ag layer thickness. Diminishing of this phase means increasingly fewer Ag atoms diffused to the ITO film with increasing Ag layer. Perhaps, the thicker Ag layer delaminates abruptly before much of the Ag layer diffuses into the ITO film. Incorporating Ag into the ITO matrix might have introduced defects (vacancy, substitutional, interstitial and grain boundary) in the ITO matrix which can be observed in the reduced ITO film quality (Table 2).

The analysis further showed that the thinner Ag layer has a relatively higher potential to impact the sample's crystal orientation properties. With the Ag layer thickness increased, the ITO film's preferential orientation was significantly altered. For the 10 nm Ag layer sample, the orientation changed from the (400) preferred orientation to that of the delafossite structure. This came

with (211) peak intensity pronounced and its width broadening. The enhanced peak intensity suggests enhanced preferential orientation to this plane, whereas, the broadening can be explained by this sample's reduced crystallite size and increased micro-strain (Table 3). The peak intensity and broadening of the (211) was reduced with Ag layer thickness increment. The ITO film quality, determined by the I(222)/I(400) peaks ratio, indicated that with a thinner Ag (10 nm) layer, the ITO film quality was reduced (Table 2). It was then enhanced again with the Ag layer thickness increment, supporting the possibility of fewer defects in the bilayer films with the Ag thickness increase. Besides, the ITO films revealed polycrystalline features of cubic bixbyite structure In_2O_3 corresponding to the JCPDS card number 06-0416 (Ait Aouaj et al. 2007, Taha et al. 2018). No exclusive Ag peak was observed for all Ag/ITO bilayer films suggesting that the Ag layer diffused into the ITO film for thinner and continued to delaminate from ITO for thicker Ag bilayer films as suggested by the AFM study.

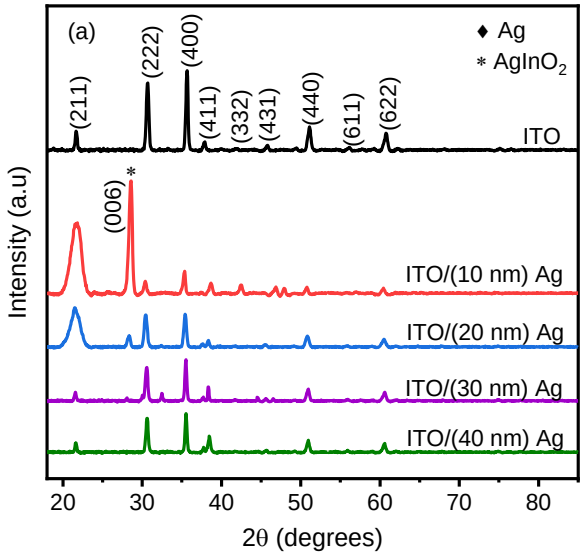

Figure 2: XRD pattern for annealed ITO and Ag/ITO bilayer films of Ag layer thickness increment

Employing the Williamson-Hall formula to the XRD data showed a more significant effect on the samples' micro-strain and crystallite size properties with the thinner Ag layer (Williamson and Hall 1953). Relative to ITO films, the analysis indicated for the thinner Ag layer (10 nm) sample, a change of tensile to compressive micro-strain and reduced crystallite size (Table 2). With the 20 nm Ag layer, the sample's compressive micro-strain decreased, changing from compressive to tensile again with the Ag layer thickness further increased. The crystallite size indicated a general increase with Ag layer thickness increments. The micro-strain and crystallite size were evaluated at the (211) peak using the Williamson-Hall (Williamson and Hall 1953) equation (1) expressed as:

$$\beta \mathrm{Cos}\theta = \frac{k\lambda}{D} + 4\varepsilon \mathrm{Sin}\theta \qquad (1)$$

where D is the crystallite size, β is the full width at half-maximum, k is the Scherer factor taken as 0.94 for spherical crystallites, λ is the x-ray wavelength, θ is the Bragg's diffraction angle, and ε is the micro-strain. The micro-strain (ε) can be obtained from the slope of $\beta\text{Cos}\theta$ against $4\text{Sin}\theta$ the plot and crystallite size (D) from its $\beta\text{Cos}\theta$-intercept.

Table 2: The crystal quality, crystallite size and micro-strain for the annealed ITO, and Ag/ITO bilayers of Ag layer thickness increment

Ag layer thickness (nm)	I(222/400)	Crystallite size (nm)	Micro-strain $\times 10^{-3}$
0	0.865	35.8	1.60
10	0.526	2.60	- 44.6
20	1.000	7.20	-7.50
30	0.835	45.1	1.60
40	0.902	38.0	1.30

Likewise, further XRD data analysis suggested that at the present annealing condition, the thinner Ag layer had a relatively higher potential to enhance the bilayer films' lattice parameters properties. Relative to the rest of the films, the thinner Ag layer thickness bilayer films showed relatively higher FWHM and lattice parameters (Table 3). The observed expanding lattice parameters relative to the ITO sample suggested a diffusion of Ag atoms with a relatively large atomic radius (0.126 nm) into the ITO matrix (Cao et al. 2010), as the XRD analysis also suggested. The parameters, however, decreased with increasing Ag layer thicknesses. The decrease in lattice parameter suggested diminishing of Ag atoms in the ITO matrix, which correlates with the increased surface delamination observed in AFM and XRD analysis. The observed lattice parameters results agreed with the observed bilayer films' peak position shifting. With the 10 nm Ag layer sample, the (222) and (400) peaks' positions shifted toward lower diffraction angles (Table 3) consistent with the observed sample's lattice expansion. The peak position, however, increasingly shifted toward a larger XRD diffraction angle with increased Ag layer thickness again consistent with the observed lattice parameters results trend. The lattice parameters (lattice constant, a and inter-planar distance, d) of (222) and (400) crystal planes were estimated using equations (2) and (3) (Cao et al. 2010) where h, k, l represent the Miller indices.

$$n\lambda = 2d\sin 2\theta \qquad (2)$$

$$a = d_{hkl}\sqrt{h^2 + k^2 + l^2} \qquad (3)$$

Table 3: Structural parameters for annealed ITO and Ag/ITO bilayer films of Ag layers thickness increment

Ag layer (nm)	Miller indices	FWHM (deg.)	Peak position (deg.)	d-spacing (Å)	a-parameter (Å)
0	(222)	0.372	30.68	2.912	10.09
10		0.383	30.38	2.939	10.18
20		0.437	30.45	2.934	10.16
30		0.369	30.55	2.924	10.13
40		0.347	30.61	2.918	10.11
0	(400)	0.321	35.65	2.517	10.07
10		0.342	35.31	2.540	10.16
20		0.293	35.42	2.532	10.13

30	0.281	35.51	2.526	10.11
40	0.280	35.53	2.525	10.10

Electrical properties

The four-point probe and Hall measurement indicated that a thinner Ag layer could have more potential to keep the rapidly annealed Ag/ITO electrical properties (Figure 3). Compared to the ITO films, the 10 nm Ag layer sample indicated a relatively higher sheet resistance (Figure 3a) with reduced Hall conductivity (Figure 3b). These changes in electrical properties can be attributed to increased grain boundary scattering, reduced carrier concentration (Figure 3c) and carrier mobility (Figure 3d). An increase in structure defects and surface roughness as the AFM results suggested, explains the carriers' properties observed. The change of micro-strain from tensile to compressive might have also contributed to these changes. At 20 nm Ag layer thickness, the annealed Ag/ITO bilayer film effect became more pronounced. The sheet resistance of the bilayer films further increased and its conductivity decreased. The further decrease in conductivity can be attributed to a further increase in surface roughness, as indicated by AFM results, which contributed to further carrier scattering, further limiting charge carrier mobility and reducing the sample's conductivity. The relatively reduced diffuse of Ag into ITO suggested in XRD results could also lead to fewer carriers contributing to this sample's conductivity.

When increasing the Ag layer thickness to 30 nm, more changes in the annealed Ag/ITO films were observed. The sheet resistance of the bilayer film further increased and its conductivity decreased. The change in the electrical properties remains primarily due to the decrease in the carrier concentration which outweighs the somewhat increase in carrier mobility (Figure 3 [c, d]). Again, further reduced Ag phase in the sample as suggested by XRD results could be a reason for the carrier concentration to decrease. Conversely, the change from compressive to tensile micro-stain for this sample reduced the density of defects in the conduction band edge, thus further lowering the carrier concentration and increasing the carrier transport. With 40 nm Ag layer the effect observed for 30 nm Ag layer bilayer films became further noticeable. The sheet resistance of the bilayer film further increased and its conductivity decreased. Similar reasons provided for the 30 nm Ag layer sample could explain the further sheet resistance increase and reduction in conductivity. A further decrease of micro-stain for this sample suggested further relaxed bilayer films that can have further effects on the carrier concentration and transport as suggested for the 30 nm Ag layer thicknesses.

The observed changes in the electrical properties of annealed Ag/ITO films disagree with those observed for similar conventionally annealed bilayers, which showed a decrease in sheet resistance with an increase in Ag layer thicknesses (Sivaramakrishnan et al. 2009). This disagreement suggested that the electrical properties of Ag/ITO films strongly depend on the annealing ramping rate.

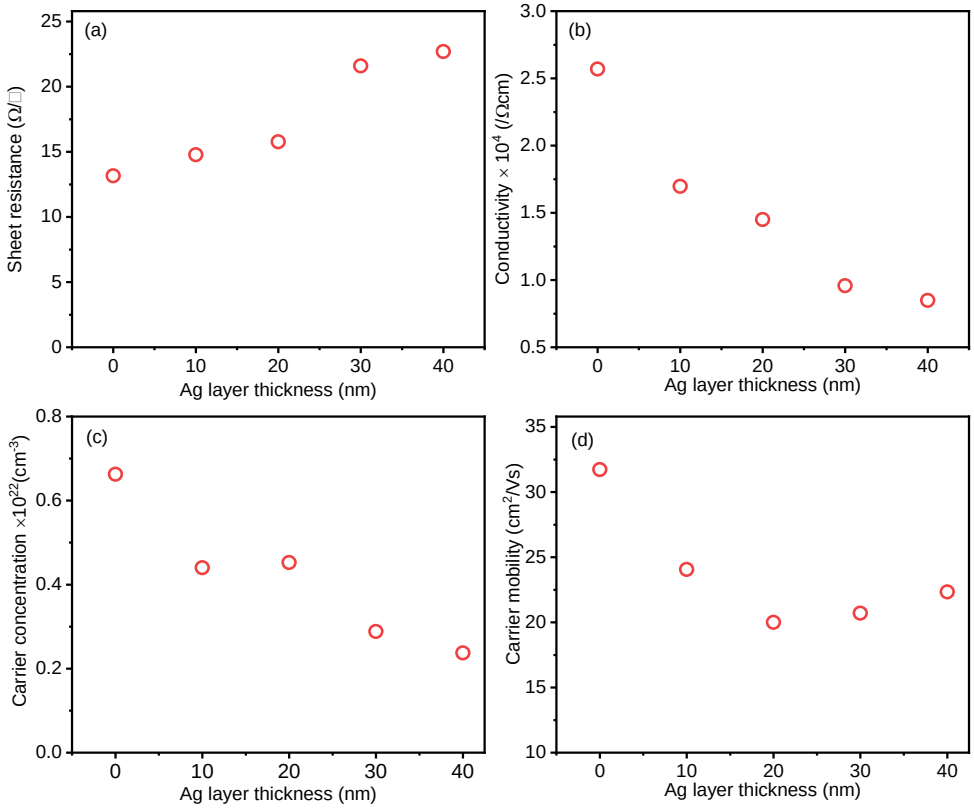

Figure 3: Sheet resistance (a), conductivity (b), Carrier concentration (c) and mobility (d) for the annealed ITO and Ag/ITO bilayer films of Ag layers thickness increment

Solar transmittance

At the present annealing conditions, the spectrophotometer measurement showed that the thinner Ag layer achieved relatively lower solar transmittance as compared to the thinner Ag layer and the ITO film. The measurement indicated a usual ITO film solar transmittance spectrum for the annealed reference sample. This sample had a relatively higher average solar transmittance (T_{sol}) of above 80% (Figure 4 b). The sample indicated transmittance spectra with oscillating patterns in the lower part of the visible spectrum (Figure 4a). This indicated a uniform thickness surface that supports constructive and destructive interference between light waves reflecting from the top and bottom surfaces of the film (Granqvist 2007). The sample also showed a steep decrease in the near-infrared (NIR) transmittance indicating this sample's high carrier concentration and mobility, as supported by the electrical measurements results (Figure 3 [c, d]). With a 10 nm Ag layer, the oscillating pattern observed in the annealed ITO film disappeared. The Ag atoms diffusing into the ITO during annealing likely disrupted the interface required for a clear interference pattern, causing the oscillations to disappear. Besides, the NIR transmittance of this sample remained almost unchanged indicating relatively maintained electrical properties of the ITO films as the electrical measurements indicated (Figure 3). The sample also maintained a relatively higher T_{sol} (Figure 4a) and T_{AVE} (Figure 4b) suggesting that thinner bilayer films can be important for applications in optoelectronics applications.

A further noticeable change was observed in the transmittance spectrum for the 20 nm Ag layer sample. The sample T_{AVE} also decreased from 80% to above 70% (Figure 4 b). Relative to the ITO film, the sample

showed reduced visible transmittance however, this time, the oscillating patterns reappeared but were modified. The reduced visible transmittance suggested that the film increasingly absorbed visible radiation in this region as the sample partly agglomerated and the surface got roughing during annealing as the AFM result suggested. Whereas, the reappearing of the oscillating patterns means, with this thickness increasing, less Ag diffused into the ITO films as suggested by XRD results (Figure 2) thus, relatively maintaining the ITO transmittance shape. The onset of agglomerating and roughing behaviour in the sample explains the modified properties of the oscillating patterns. This sample indicated further reduced T_{AVE} due to the reduced visible transmittance.

At the 30 nm Ag layer, the annealed Ag/ITO film transmittance spectrum features significantly changed. The visible and lower part of NIR transmittance decreased, whereas, the higher part of NIR transmittance relatively increased with the oscillating pattern disappearing again. Probably, the 30 nm layer is thick enough to undergo more pronounced morphological changes including increased crystallized structure and delaminated surface as suggested by the XRD (Table 2) and AFM (Figure 1 [g, h]) results, respectively. These changes disrupt the regular shape and oscillating pattern in the visible spectrum. Additionally, an increase in the higher part of NIR transmittance suggested a relatively reduced carrier concentration and possibly lower mobility, as supported by the electrical measurements (Figure 3[c, d]). On average, the transmittance of this sample was further reduced to about 60 %.

Increasing the Ag layer to 40 nm, the sample regained the ITO film's solar transparent (T_{sol}) spectra shape, however, with the NIR transmittance increased (Figure 4 a). The sample's T_{AVE} increased from 55% to above 75% (Figure 4 b). The delaminating pattern suggested by AFM results (Figure 1 [j-k]) is also supported by the XRD results by the absence of the Ag phase in the samples (Figure 2), might have caused the sample to mimic the reference sample shape. The increase in the NIR transmittance signifies a reduced electrical conductivity due to a huge disruption of electrical continuity in the film's surfaces as suggested by electrical properties results (Figure 3 c).

The average solar transmittance, T_{AVE} values for these samples' solar transmittance spectra, $T(\lambda)$ were computed using Air Mass 1.5 solar irradiance, $G(\lambda)$ (U.S. Department of Energy (DOE)/NREL/ALLIANCE 1999) based on the relation;

$$T_{AVE} = \frac{\int_{250}^{2500} G(\lambda)T(\lambda)d\lambda}{\int_{250}^{2500} G(\lambda)d\lambda} \qquad (6)$$

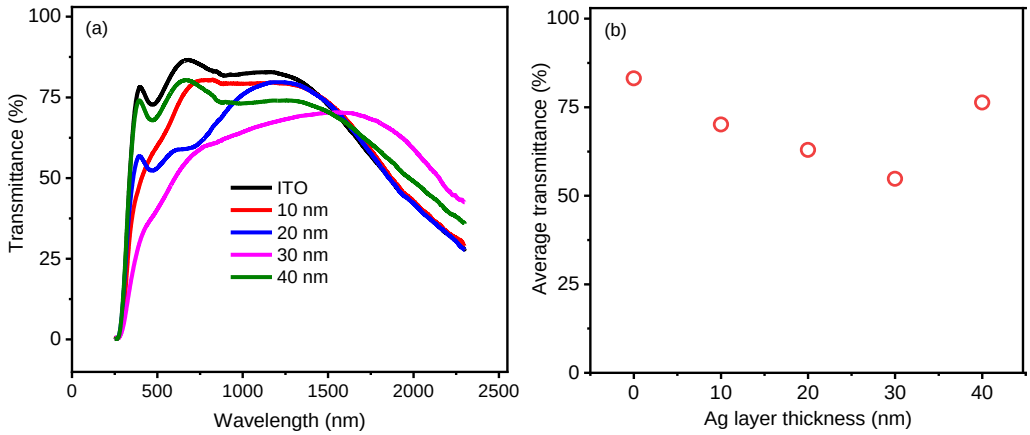

Figure 4: Solar transmittance spectra (a) with corresponding average solar transmittance (b) for the annealed ITO and Ag/ITO bilayer films of Ag layer thickness increment

Optical Bandgap

The Tauc-plots extrapolates indicated a potential for bandgap narrowing for thinner Ag layer and broadening for thicker Ag/ITO bilayer films. The annealed Ag/ITO with a 10 nm Ag layer showed changes in the sample's bandgap. Relative to the ITO film, the analysis showed a reduced bandgap (Figure 5 [a, b]). The reduced bandgap suggested that during annealing, Ag atoms diffused into the ITO medium, introducing some defects into the sample. These defects reduced the bandgap by creating levels near the conduction or valence bands. This introduced a localised energy state narrowing the bandgap. Furthermore, the increased micro-stain observed in this sample could alter the atomic spacing, leading to a reduced bandgap. The bandgap continued to decrease as the sample's Ag layer increased to 20 nm. The reason for this includes increased roughing of the sample surface, as suggested by the AFM results (Table 1). Roughing of the sample surface usually forms more surface defects, which can introduce localised states within the bandgap. These defects perhaps allowed electrons to transit at lower energies, effectively narrowing further the bandgap.

Compared to 10 nm and 20 nm Ag layer samples, the 30 and 40 nm samples indicated relatively larger bandgap as compared to the ITO film. The 30 nm Ag layer sample's bandgap increased as compared to the ITO films. At this thickness and annealing conditions, the sample has started to delaminate, as suggested by the AFM and Ag atoms and diffusing into the ITO had greatly reduced, as indicated by the XRD results. The sample's crystallite size has increased as the XRD result also suggests. These combined likely introduced fewer defect states in the sample, which caused a subsequent increase in the bandgap. With a 40 nm Ag layer, the delaminating behaviour has matured as suggested by both AFM and transmittance measurements. The diffusion of Ag atoms into the ITO is even more limited as indicated by the XRD results. The crystallite size remained larger, and the tensile strain was reduced, indicating a more relaxed structure. As a result, the bandgap increased further compared to the 30 nm sample. Compared to the ITO reference sample, the bandgaps for the 30 nm and 40 nm Ag layer samples were unexpectedly larger. This can be attributed to the enhanced crystallite size of these samples as suggested by the XRD results. The observed bandgap for the samples was (Figure 5 [a, b]) within the reported ITO thin films bandgap (3.38 - 4.15 eV) (Guillén and Herrero 2006, Parida et al. 2019).

The bilayer films' optical bandgaps were estimated using equation (7) that relates the direct bandgap, E_g and absorption. α of the films (Guillén and Herrero 2006).

$$(\alpha h\nu)^2 = \beta(h\nu - E_g) \qquad (7)$$

where $h\nu$ represents photon energy and α can be computed using solar transmittance, $T(\lambda)$ and the film thickness, *t*, from the relation $T(\lambda) = A\exp(\alpha t)$. By extrapolating equation (7) plots' linear part to $(\alpha h\nu)^2 = 0$ the optical band gaps can be estimated.

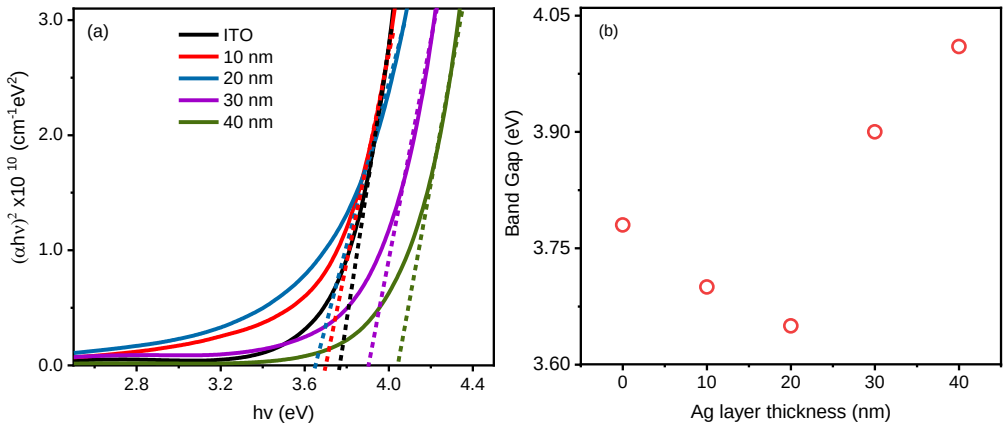

Figure 5: Tauc plot extrapolates (a) with corresponding estimated bandgaps (b) for the annealed ITO and Ag/ITO bilayers films with Ag layer thickness increment

Conclusion

The present work revealed Ag/ITO bilayer films of thinner Ag layer thickness achieved bilayer film properties with optoelectronics applications' potential use. These films showed relatively stable surfaces with fewer high peaks/valleys and normally distributed roundish grains. Systematic increments in Ag layer thickness transformed the bilayer films' surfaces from roundish grains to bulged grains then to sharper smaller grains then to a more uniform surface with fewer large protruding features. The inclusion of the Ag layer on ITO films enhanced the bilayer films' grain sizes and surface roughness. The 10 nm Ag layer changed the ITO film crystal preferential orientation to the delafossite structure of $AgInO_2$ which diminished and disappeared with Ag layer thickness increment. With a thinner Ag layer, the ITO film's quality was strongly reduced, and then recovered with Ag layer thickness increment, although in different preferential orientation. Bilayer film with this thickness exhibited ITO film micro-strain transformed from tensile to compressive, reducing its crystallite size. With the Ag layer thickness increment, the micro-strain transformed from compressive to tensile again. The 10 nm Ag bilayer thickness bilayer film showed a relatively large lattice expansion which shrunk with Ag layer thickness increment.

The 10 nm Ag layer thickness bilayer films showed relatively higher electrical conductivity due to higher carrier mobility and carrier concentration. Ag layer thickness increment, however, recorded conductivity decrease contrary to the expected. Thicker Ag layer bilayer films had relatively higher T_{sol}, however, with other optoelectronic properties limited. The bilayer films indicated bandgaps within the reported ITO thin films bandgap (3.38 - 4.15 eV). Thinner Ag layer bilayer films provided relatively good adhesion of the Ag layer on ITO films, average solar transmittance of 76 % and relatively lower sheet resistance of $13.2\Omega/\square$ potential for optoelectronics applications. This study extends the potential use of Ag/ITO bilayer films in optoelectronic applications, viz.

bifacial CZTS solar cells' back contact, requiring present processing conditions.

Acknowledgement

This work was supported by the University of Dar as Salaam; Mkwawa University College of Education, the International Science Program (ISP)-at Uppsala University, Sweden and the University of Pretoria, South Africa.

Declarations

Funding:

Mkwawa University College of Education, University of Dar es Salaam; Tanzania.

International Science Program (ISP)-Uppsala University, Sweden.

Clean and Green Energy, Department of Physics, University of Pretoria, South Africa.

Conflicts of interest/Competing interests:

The authors declare that there is no conflict of interest or competing interests.

References

Ait Aouaj M, Abd-Lefdil M, Cherkaoui El Moursli F and Hajji F 2007 Ag/ITO transparent conducting oxides. *Eur. Phys. J. Appl. Phys.* 40 (1): 55–58.

Cao C-B, Xiao L, Song X-P and Sun Z-Q 2010 Influence of annealing and Ag doping on structural and optical properties of indium tin oxide thin films. *J. Vac. Sci. Technol. A Vacuum, Surfaces, Film.* 28 (1): 48–53.

Cui H, Liu X, Liu F, Hao X, Song N and Yan C 2014 Boosting Cu2ZnSnS4 solar cells efficiency by a thin Ag intermediate layer between absorber and back contact. *Appl. Phys. Lett.* 104 (4): 2–6.

Ge J, Chu J, Yan Y, Jiang J and Yang P 2015 Co-electroplated Kesterite Bifacial Thin-Film Solar Cells: A Study of Sulfurization Temperature. *ACS Appl. Mater. Interfaces* 7 (19): 10414–10428.

Ge J, Yu Y, Ke W, Li J, Tan X, Wang Z, Chu J and Yan Y 2016 Improved performance of electroplated CZTS thin-film solar cells with bifacial configuration. *ChemSusChem* 9 (16): 2149–2158.

Granqvist CG 2007 Transparent conductors as solar energy materials: A panoramic review. *Sol. Energy Mater. Sol. Cells* 91 (17): 1529–1598.

Granqvist CG and Hultåker A 2002 Transparent and conducting ITO films: New developments and applications. *Thin Solid Films* 411 (1): 1–5.

Guillén C and Herrero J 2006 Influence of oxygen in the deposition and annealing atmosphere on the characteristics of ITO thin films prepared by sputtering at room temperature. *Vacuum* 80 (6): 615–620.

Guillén C and Herrero J 2015 Surface-properties relationship in sputtered Ag thin films: Influence of the thickness and the annealing temperature in nitrogen. *Appl. Surf. Sci.* 324: 245–250.

Han H, Mayer JW and Alford TL 2006 Effect of various annealing environments on electrical and optical properties of indium tin oxide on polyethylene napthalate. *J. Appl. Phys.* 99 (12): 123711.

Kim HC, Alford TL and Allee DR 2002 Thickness dependence on the thermal stability of silver thin films. *Appl. Phys. Lett.* 81 (22): 4287–4289.

Kim J-S, Kang J-K and Hwang D-K 2016 High efficiency bifacial $Cu_2ZnSnSe_4$ thin-film solar cells on transparent conducting oxide glass substrates. *APL Mater.* 4 (9): 096101.

Lee CH, Park JS and Seong TY 2013 Dependence of thickness and temperature on the thermal stability of Ag films deposited on GaN layers for vertical-geometry GaN-based light-emitting diodes. *Superlattices Microstruct.* 61: 160–167.

Mirzaee M and Dolati A 2014 Effect of content silver and heat treatment temperature on morphological, optical, and electrical properties of ITO films by sol–gel technique. *J. Nanoparticle Res.* 16 (9): 2582.

Mwakyusa LP, Leist L, Rinke M, Welle A, Paetzold UW, Richards BS and Hetterich M 2020 Impact of silver incorporation at the back contact of Kesterite solar cells on structural and device properties. *Thin Solid Films* 709 (2020): 138223.

Ollotu ER, Nyarige JS, Mlyuka NR, Samiji ME and Diale M 2020 Properties of ITO thin films rapid thermally annealed in different exposures of nitrogen gas. *J. Mater. Sci. Mater. Electron.* 31 (19):

16406–16413.

Parida B, Gil Y and Kim H 2019 Highly Transparent Conducting Indium Tin Oxide Thin Films Prepared by Radio Frequency Magnetron Sputtering and Thermal Annealing. *J. Nanosci. Nanotechnol.* 19 (3): 1455–1462.

Sivaramakrishnan K, Ngo AT, Iyer S and Alford TL 2009 Effect of thermal processing on silver thin films of varying thickness deposited on zinc oxide and indium tin oxide. *J. Appl. Phys.* 105 (6): 063525.

Song S, Yang T, Liu J, Xin Y, Li Y and Han S 2011 Rapid thermal annealing of ITO films. *Appl. Surf. Sci.* 257 (16): 7061–7064.

Taha H, Jiang Z-T, Henry DJ, Amri A, Yin C-Y, Alias AB and Zhao X 2018 Improved mechanical properties of sol-gel derived ITO thin films via Ag doping. *Mater. Today Commun.* 14: 210–224.

U.S. Department of Energy (DOE)/NREL/ALLIANCE 1999 Solar Spectral Irradiance: Air Mass 1.5

Williamson GK and Hall WH 1953 X-ray line broadening from filed aluminium and wolfram. *Acta Metall.* 1 (1): 22–31.